

Article

Effect of Cr Doping Concentration on the Structural, Optical, and Electrical Properties of Lead Sulfide (PbS) Nanofilms

Jiabin Huo ¹, Wei Li ^{1,*} and Teng Wang ²

¹ Guangdong Engineering Technology Research Center of Efficient Green Energy and Environmental Protection Materials, School of Physics and Telecommunication Engineering, South China Normal University, Guangzhou 510006, China; 2017021660@m.scnu.edu.cn

² School of Computer, South China Normal University, Guangzhou 510631, China; wangteng@m.scnu.edu.cn

* Correspondence: liwei@m.scnu.edu.cn

Received: 14 May 2019; Accepted: 4 June 2019; Published: 10 June 2019



Abstract: In this paper, pristine and Cr-doped lead sulfide (PbS) nanofilms were prepared by chemical and deposition methods. From X-ray diffraction (XRD) analysis, all nanofilm samples possessed good crystallinity with a preferential orientation of the (200) crystal plane. As the Cr doping concentration increased, the nanofilm grain size decreased from 71.5 to 18.9 nm. The SEM results revealed that the variation in Cr concentration led to different grain shapes, and the grain size became smaller with the increasing doping concentrations. Optical studies showed that the optical band gap of PbS films increased from 1.21 to 1.60 eV after Cr doping due to the quantum confinement effect; the 2% Cr-doped PbS nanofilm, with an E_g of 1.49 eV, matched the ideal band-gap value. The electrical characterization showed that, for a 2% Cr doping concentration, the Hall mobility and volume carrier concentration of the nanofilm reached the maximum values of $59.6 \text{ cm}^2 \cdot \text{V}^{-1} \cdot \text{s}^{-1}$ and $20.7 \times 10^{16} \text{ cm}^{-3}$ respectively. The 2 at.% Cr-doped PbS nanofilms exhibited the best optical and electrical properties, suitable for solar cell applications.

Keywords: PbS; nanofilms; band gap; Cr

1. Introduction

Thin film materials are the predominant materials utilized in vacuum, microelectronics, and materials science due to their unique and excellent properties. As an IV–VI semiconductor elemental compound, PbS has a small direct band gap (~ 0.4 eV at room temperature) [1,2] and a relatively large excitation Bohr radius (approximately 18 nm). Its optical band gap is adjustable [3] and combines with high temperature and oxidation resistance [1,4]. To date, PbS thin films are widely used in the field of optical and electronic devices due to their high response rates [1,5], ease of preparation, and stable operation at room temperature.

Doping is an effective control technique to adjust particle size, surface morphology, and crystal structure [6]. During film synthesis, doping improves the physical and chemical properties of the film [7]. Doping with Cr effectively increases the optical band gap of semiconductor materials, broadens the light response range, inhibits the electron hole in the compound, and improves the semiconductor surface activity [3]; as a result, it is widely used as a doping agent.

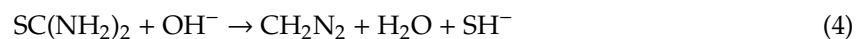
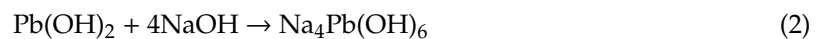
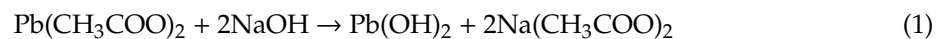
In order to apply PbS films to the solar energy field, we prepared PbS films using chemical bath deposition (CBD) [8], successive ionic layer adsorption and reaction (SILAR) [9], spray pyrolysis [10], vacuum evaporation [11], pulsed laser deposition [12], electrodeposition [13], and other techniques. In this paper, Cr-doped and undoped PbS films were prepared by CBD. CBD does not require complicated equipment [14] and the process is simple. It can grow large-area films [15], while remaining

an environmentally friendly and non-polluting preparation method; compared with other methods, CBD could be readily adapted industrially [16].

To the best of our knowledge, there are few reports on the preparation of Cr-doped PbS films by chemical and deposition methods. In this novel research, the effects of Cr doping on the microstructure, surface morphology, and optical and electrical properties of PbS films were investigated; the optimal doping amount was determined to improve the applicability of PbS nanofilms in solar cell absorbing materials [17].

2. Materials and Methods

All reagents purchased were analytical grade and used without further purification. Microscope glass slides (75 mm × 25 mm × 1 mm) were used as substrates. Deposition of lead sulfide film was accomplished by immersion in a chemical bath deposition solution prepared from 0.09 M lead acetate, 0.5 M sodium hydroxide, and 0.45 M thiourea. The total reaction volume was adjusted with deionized water to 100 mL. The pH was adjusted to 12 by adding NaOH to the reaction bath, and the solution temperature was kept at 70 °C. The cleaned glass substrate was vertically dipped into the beaker containing the reaction solution and removed after 40 min. It was finally cleaned with deionized water and dried at room temperature. The chemical process for preparing the PbS film was as follows:



Similarly, by adjusting the initial molar ratio of chromium chloride to lead acetate ([Cr/Pb] = 1, 2, 3, 4, and 5 at.%), the overall chemical reaction became the following:



The structural, optical, and electrical properties of the nanofilms were systematically analyzed. An X-ray diffractometer (Philips X'pert, Malvern, UK) using Cu K α radiation ($\lambda = 1.5406$) was employed to study the structural characteristics of the films. The surface morphologies and elemental compositions of the films were characterized by a scanning electron microscope (ZEISS Ultra 55, Oberkochen, Germany) with an attached energy-dispersive X-ray spectroscope (EDX). The optical properties of films were measured using a PerkinElmer Lambda 950 ultraviolet–visible–near-infrared (UV–Vis–NIR, Waltham, MA, USA) spectrophotometer. A Hall effect tester (RH2053, PHYS TECH GmbH, Moosburg, Bavaria, Germany) was used to determine the Hall mobility, carrier concentration, and resistivity of the nanofilms.

3. Results and Discussion

3.1. Structural Properties

In order to investigate the effect of Cr dopant on the structural properties of the PbS nanofilms, crystal structures of pure and Cr-doped PbS nanofilms were studied by X-ray diffraction (XRD), with a diffraction angle scanning range from 10° to 90°. Figure 1a shows the XRD patterns of pure PbS film and x at.% Cr-doped PbS thin films ($x = 1, 2, 3,$ and 4). All nanofilms showed characteristic peaks corresponding to the crystal plane orientation of (111), (200), (220), (311), (222), (400), (331), (420), (422), and (511) which precisely coincide with PbS (JCPDS: 05-0592). Moreover, no impurity peaks were observed, indicating the prepared samples were pure FCC PbS. These results are similar to other

PbS-doped films using other ions [17,18]. The shape of the diffraction peak was sharp, indicating good polycrystalline film structure. Figure 1 shows that the preferential growth direction of the deposited lead sulfide films was (200). However, Cr doping changed the structural properties of the PbS films. Firstly, the peak strengths of (111) and (200) after Cr doping decreased significantly relative to pure PbS films, which may be related to the structural disorder caused by Cr doping [19]. There is a small shift in the Bragg angles of PbS (111) and (200) toward higher values (from 25.971° and 30.060° for pure PbS to 26.045° and 30.167° for 5% Cr-doped PbS nanofilms, respectively), as seen in Figure 1b. This implied a change in the lattice constant upon Cr doping and suggests that Cr³⁺ ions replace Pb²⁺ ions in the lattice due to their small ionic radius (the radius of the Cr³⁺ ion is 0.069 nm) compared to that of Pb²⁺ (0.119 nm). These results agree with previous literature reports [6]. The intensity of the (111) and (200) peaks increased as the Cr concentration increased. When the Cr concentration exceeded 2%, the intensity of the peak decreased with increasing Cr concentration. Figure 2g clearly illustrates the Cr distribution in the nanofilm sample. Therefore, we think that the Cr³⁺ ion amorphyously adhered to the PbS crystal as the doping amount increased. On the surface, these attached ions can hinder additional crystal growth. In addition, grain size reduction (shown in Table 1) also prevented Cr³⁺ ions from entering the crystal; thus, the optimal doping amount should be considered when doping the crystal.

Scherrer's Equation [20],

$$D = 0.94\lambda / \beta \cos \theta \quad (7)$$

can be used to calculate the grain size of PbS nanofilm samples (θ is the Bragg diffraction angle, β is the full-width at half-maximum (FWHM), and λ is the X-ray radiation wavelength). Table 1 shows that the nanofilm grain sizes decreased with increasing Cr doping levels. As observed in Figure 1b, the shape of the XRD line indicated a significant broadening after doping due to a grain size decrease with increasing Cr doping, which broadened the diffraction peak of the PbS film. Preetha believes that, as the relative concentration of Cr decreases, the grain size increases; this observation is in good agreement with our experimental results [1]. Equation (8) [21],

$$\varepsilon = \beta \cos \theta / 4 \quad (8)$$

can be used to calculate the microstrain values of undoped and Cr-doped PbS nanofilm samples. Table 1 summarizes the calculated microstrain values which increased with the increased Cr doping. It is well known that a lower microstrain value corresponds to a higher grain size with fewer structural defects. In general, when ions with a smaller ionic radius (such as Cr³⁺) replace those with a larger ionic radius (such as Pb²⁺), lattice shrinkage will occur. Therefore, as a result of lattice shrinkage and strain increase, the grain size of the sample decreased as the Cr doping amount increased. Dislocation density is defined as the length of dislocation lines per unit volume of the crystal. The dislocation density can be calculated using the following formula [21]:

$$\rho = 15\varepsilon / aD \quad (9)$$

where D is average crystallite size and ε is the strain. Table 1 lists the calculated dislocation densities which increased with increasing Cr doping amounts. The dislocation density increase indicates a reduction in grain size and crystallinity. The increase in dislocation density increases the pinning effect on surface atomic motion and inhibits grain growth. At the same time, additional dislocations also provide more energy-friendly locations for nucleation, increasing the number of nucleation sites. Therefore, as the dislocation density increases, the crystal grains become finer and the crystallinity deteriorates. The standard lattice constants and lattice spacing values for undoped and Cr-doped PbS thin film (hkl) orientations are given in Table 1. Crystal plane spacing values can be calculated using the following formula [22]:

$$2d_{hkl} \sin \theta = n\lambda \quad (10)$$

where $n = 1$, $\lambda = 1.54056$ is the wavelength of the X-ray, and θ is the diffraction angle. We observed that the calculated plane spacing value and the lattice constant match the card JCPDS: 05-0592. The calculated interplanar spacing and lattice constant decreased with increased Cr doping, which may be due to lattice compression caused by crystallization and stress.

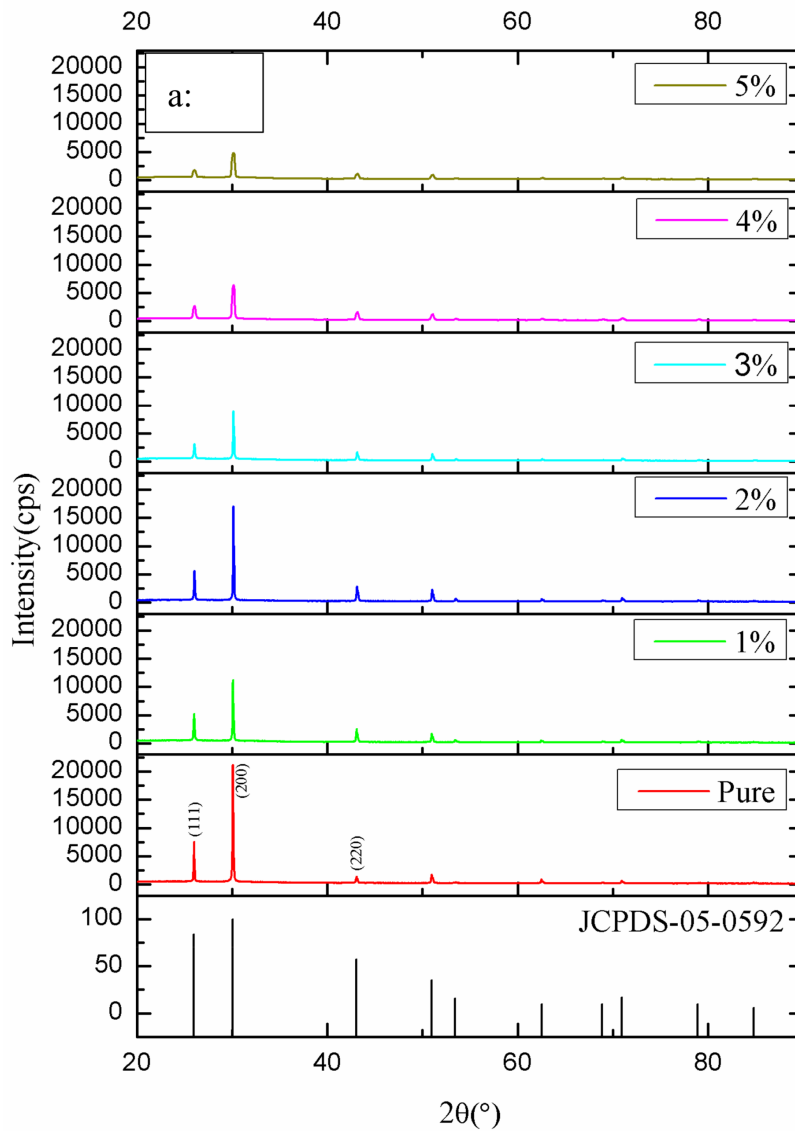


Figure 1. Cont.

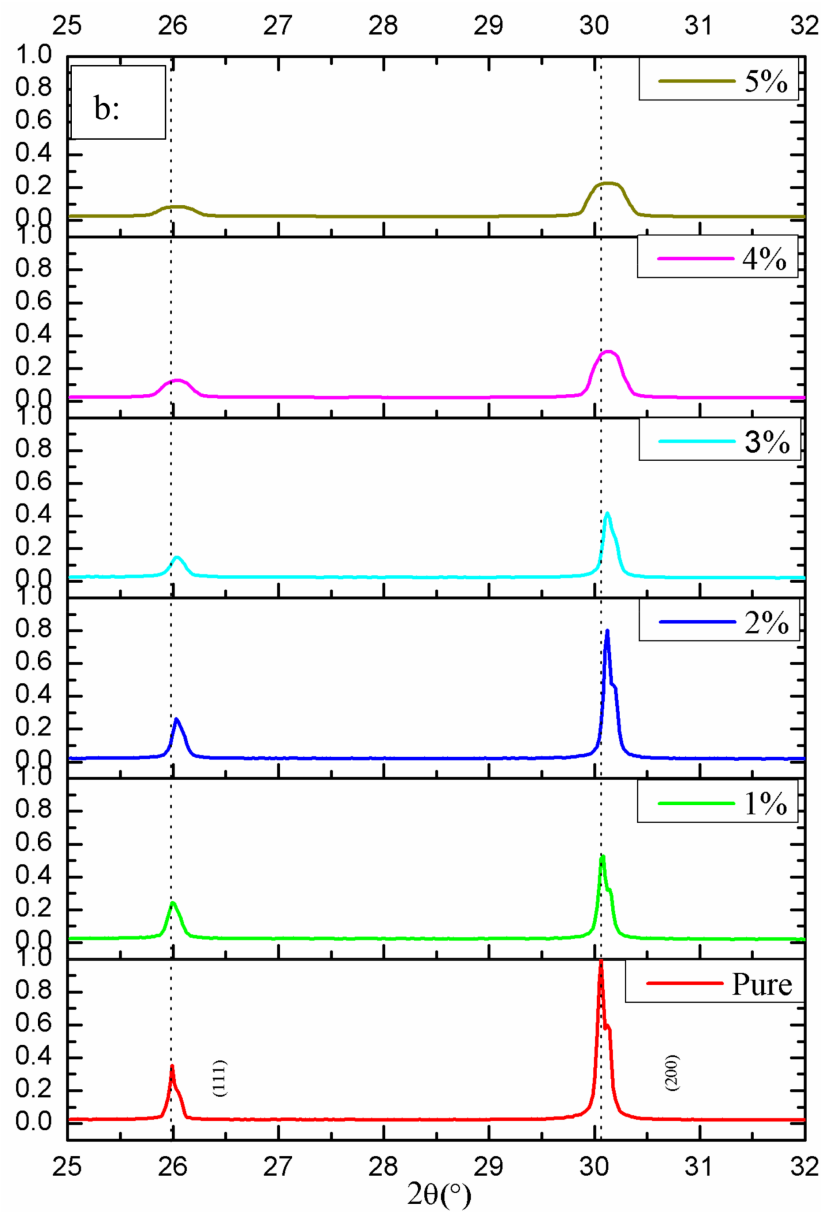


Figure 1. (a) X-ray diffraction (XRD) patterns of pure and Cr-doped lead sulfide (PbS) films; (b) shifts in the 2θ value of Cr-doped PbS thin films.

Table 1. Structural parameters of pure and Cr-doped lead sulfide (PbS) thin films obtained by X-ray diffraction (XRD) spectra. FWHM—full-width at half-maximum.

| Cr Content (at.%) | (hkl) | 2θ (°) | FWHM (radian) | Crystallite Size D (nm) | Microstrain ($\epsilon \times 10^{-3}$) | Dislocation Density (ρ) | d -Values (Å) | Lattice Parameter (Å) |
|-------------------|-------|---------------|---------------|---------------------------|---|--------------------------------|-----------------|-----------------------|
| 0 | 111 | 25.971 | 0.002234 | 63.7 | 0.544 | 2.47 | 3.42797 | 5.93742 |
| | 200 | 30.06 | 0.002007 | 71.5 | 0.485 | 1.95 | 2.97033 | 5.94066 |
| | 220 | 43.081 | 0.003176 | 46.9 | 0.739 | 4.54 | 2.09795 | 5.93389 |
| 1 | 111 | 26.02 | 0.002374 | 60 | 0.578 | 2.78 | 3.42162 | 5.92643 |
| | 200 | 30.081 | 0.002496 | 57.5 | 0.603 | 3.02 | 2.9683 | 5.93661 |
| | 220 | 43.081 | 0.004868 | 20.6 | 1.132 | 10.067 | 2.09795 | 5.93389 |
| 2 | 111 | 26.026 | 0.002688 | 52.9 | 0.655 | 3.57 | 3.42085 | 5.92509 |
| | 200 | 30.124 | 0.002618 | 54.8 | 0.632 | 3.32 | 2.96416 | 5.92833 |
| | 220 | 43.124 | 0.005236 | 18.5 | 1.217 | 12.34 | 2.09596 | 5.92826 |

Table 1. Cont.

| Cr Content (at.%) | (hkl) | 2 θ (°) | FWHM (radian) | Crystallite Size <i>D</i> (nm) | Microstrain (ϵ) $\times 10^{-3}$ | Dislocation Density (ρ) | <i>d</i> -Values (Å) | Lattice Parameter (Å) |
|-------------------|-------|----------------|---------------|--------------------------------|---|--------------------------------|----------------------|-----------------------|
| 3 | 111 | 26.033 | 0.004869 | 29.2 | 1.186 | 11.71 | 3.41995 | 5.92352 |
| | 200 | 30.126 | 0.00356 | 40.3 | 0.86 | 6.15 | 2.96397 | 5.92794 |
| | 220 | 43.129 | 0.005236 | 18.3 | 1.217 | 12.33 | 2.09572 | 5.9276 |
| 4 | 111 | 26.042 | 0.007121 | 20 | 1.734 | 25.04 | 3.41878 | 5.92151 |
| | 200 | 30.142 | 0.005236 | 27.4 | 1.264 | 13.3 | 2.96244 | 5.92487 |
| | 220 | 43.143 | 0.008238 | 18.1 | 1.915 | 30.53 | 2.09508 | 5.92577 |
| 5 | 111 | 26.045 | 0.009023 | 15.8 | 2.198 | 40.2 | 3.4184 | 5.92084 |
| | 200 | 30.167 | 0.00765 | 18.9 | 1.538 | 19.68 | 2.96004 | 5.92007 |
| | 220 | 43.145 | 0.009372 | 15.9 | 2.179 | 39.52 | 2.09498 | 5.92551 |

3.2. Morphological Properties

Figure 2 shows the surface morphology as studied by SEM for all PbS nanofilms. According to Figure 2a, nanocrystals on the surface of pure PbS films exhibit pyramidal shapes with a preferential orientation along the (200) surface. Figure 2b–f clearly show the modulation of average grain size and shape with Cr incorporation. The morphological change process is as follows: as shown in Figure 2b, the grain shape is slightly modified and morphs from the original pyramid shape to a square-like shape when the concentration of Cr is 1%. Figure 2c–e feature the SEM micrographs obtained for Cr-doped (2, 3, and 4 at.%) PbS nanofilms; the grain continues to become more square-like. In comparison to the SEM micrograph of undoped film, small grains appear on the surface. This is due to an increase in the nucleation rate rather than the growth rate due to a large number of nucleation centers [23]. Finally, as seen from Figure 2f, the grain shape continues to be modified and small particles agglomerate; the grain shape eventually becomes more complex spherical particles. The increasing doping ions provide more favorable energy positions for nucleation due to the increase in doping concentration. Ease of nucleation results in the formation of fine and dense crystal nuclei. Those crystal nuclei may agglomerate, resulting in the formation of small, dense particles that increase the continuity and uniformity of the film surface. Moreover, the size of the nanospheres decreased with increased Cr doping, and was consistent with the average particle size of the particles estimated by the XRD data and agreed with a previous report on Ag incorporation into PbS films [4]. In addition, the surface morphology of all nanofilms was smooth, dense, and free of defects or cracks. The film had good adhesion, and the results are consistent with the XRD crystal size calculation results.

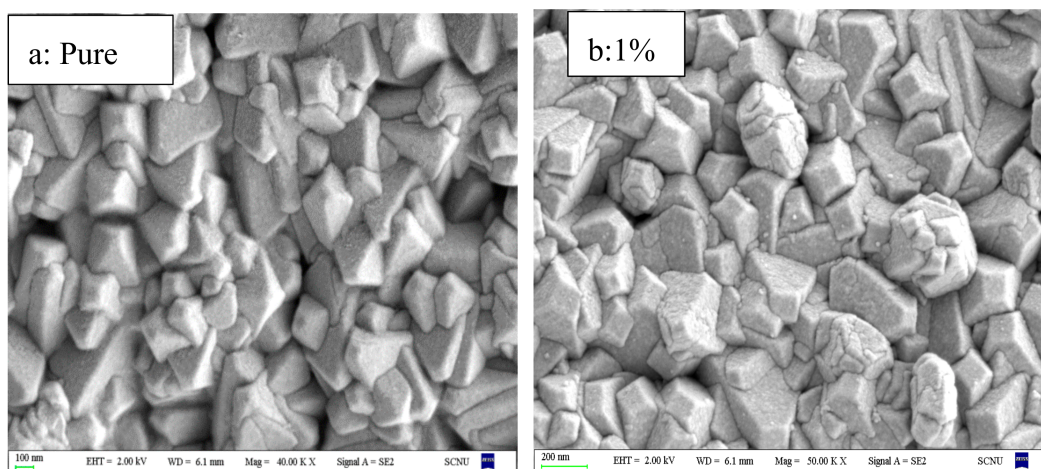


Figure 2. Cont.

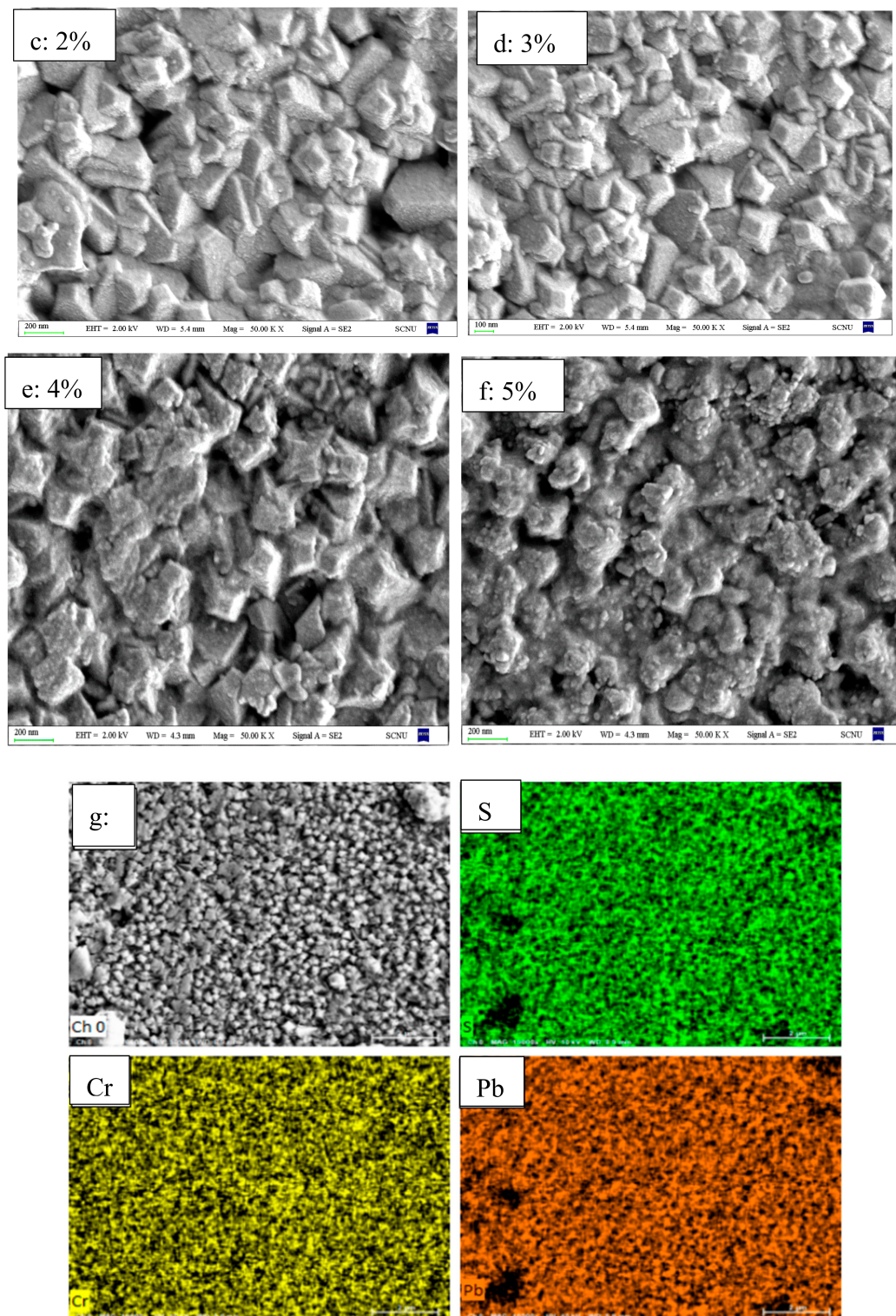


Figure 2. SEM micrographs for (a) undoped and Cr-doped (b: 1%, c: 2%, d: 3%, e: 4%, and f: 5%) PbS films; (g) energy-dispersive X-ray spectroscopy (EDS) elemental mapping of Pb, Cr, and S for the 5% Cr-doped film.

Elemental composition of the films was analyzed with energy-dispersive X-ray (EDX). The obtained EDX spectra are shown in Figure 3 which shows that Pb, S, and Cr were the only atoms present in the films, indicating the purity of the chemically deposited Cr:PbS thin films. We concluded that we obtained the expected films.

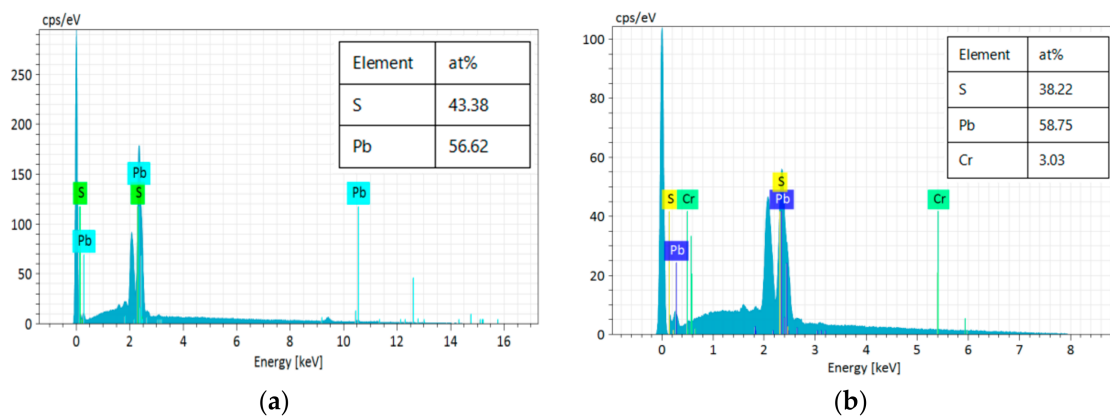


Figure 3. EDS of pristine PbS films (a) 0 at.% Cr-doped PbS film, and (b) 5 at.% Cr-doped PbS film.

3.3. Optical Research

The influence of Cr dopant on the optical properties of PbS films was studied using optical absorption and transmission spectra. The optical absorption and transmission spectra of the samples were studied by UV–Vis spectrophotometry. Figure 4 shows the optical transmission spectra of pure and Cr-doped PbS nanofilms. For undoped PbS films, the transmittance was lower in the visible region; this transmission decrease may be due to stronger absorbance by these films. The incorporation of Cr had a significant effect on the optical properties of PbS films. In Figure 4, the transmittance of the PbS films increased with increasing Cr doping amounts. This behavior can be attributed to an increased in light scattering loss. Moreover, after Cr inclusion into the film, the absorption edge was blue-shifted from near-infrared toward the visible region; this was consistent with previous reports [4,24]. Then, the absorption data of light was processed using the Tock formula [25] as follows:

$$\alpha \hbar\nu = A_0(\hbar\nu - E_g)^n \quad (11)$$

where $\hbar\nu$ is the photon energy and A_0 is a constant; for direct transition, $n = 1/2$ because lead sulfide is a direct band-gap semiconductor [3], while α is the optical absorption coefficient and can be obtained by the following formula [26]:

$$\alpha = \frac{1}{t} \ln\left[\frac{(1-R)^2}{T}\right] \quad (12)$$

where t is the thickness of the film, R is the reflectance of the film, and T is the transmittance of the film. The E_g values were obtained by extrapolating the linear portion of the plots $(\alpha \hbar\nu)^2$ vs. $\hbar\nu$ to $\alpha = 0$ [3]. Figure 5 shows the $(\alpha \hbar\nu)^2 = f(\hbar\nu)$ curve of pure and Cr-doped PbS nanofilms; the intercept of the tangent of the absorption curve on the $\hbar\nu$ axis is the band-gap value. From Figure 5, the band-gap values of lead sulfide films doped with Cr (from 0–5%) are observed, and the calculated value of the band gap of pure PbS film was 1.21 eV. Our results showed that the optical band gap of PbS film samples increased from 1.21 to 1.60 eV with increasing Cr doping amounts. A similar experimental phenomenon was reported in previous literatures [6,27]. This phenomenon is primarily due to the incorporation of Cr^{3+} ions and the decrease in grain size. Table 1 shows a clear inverse relationship between the grain size and the band gap of lead sulfide films. This may be due to the quantum confinement effect in nanocrystalline PbS films [28]. If the particle size of the nanofilm is equal to or smaller than the diameter of its Bohr excitons, the band gap of the film increases as the grain size decreases due to the quantum confinement of electrons and holes. The absorption spectral response blue-shifts, as seen in Figure 6, and this effect is covered in most nanomaterial reports [4,6]. In addition, defects may occur on the surface of the film after doping with Cr^{3+} ions. These defects promote the increase of trap states and surface states of the films. Thus, it helps increase the electron transition barrier and leads to an increase in the band gap. The results of Preetha show that, after the Cr is doped

into PbS film, the band-gap width shows a significant blue shift, consistent with our experimental results [1]. However, unlike our Cr doping experiments, the chromium concentration in literature is too high and is not an ideal dopant. Moreover, that report did not analyze the band-gap changes caused by different doping ratios [1]. Therefore, doping PbS thin films with Cr³⁺ ions is an effective method to increase the optical band gap. In particular, a 2% Cr-doped PbS film with an E_g of 1.49 eV matched well with the optimum value of the theoretical band gap (1.5 eV) previously reported [4], which can better absorb the visible to near-infrared sunlight and convert solar energy into electric energy.

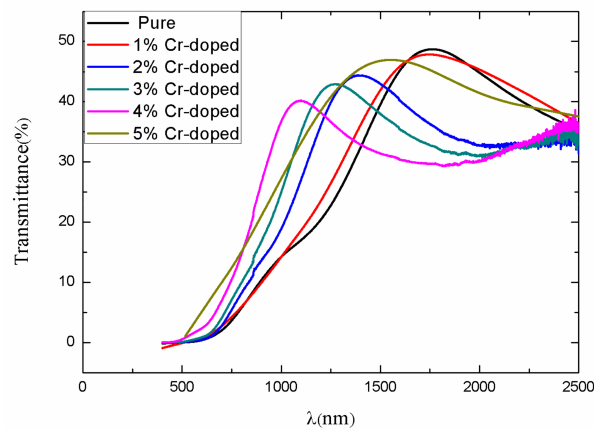


Figure 4. The optical transmittance spectra of the pure and Cr-doped PbS thin films.

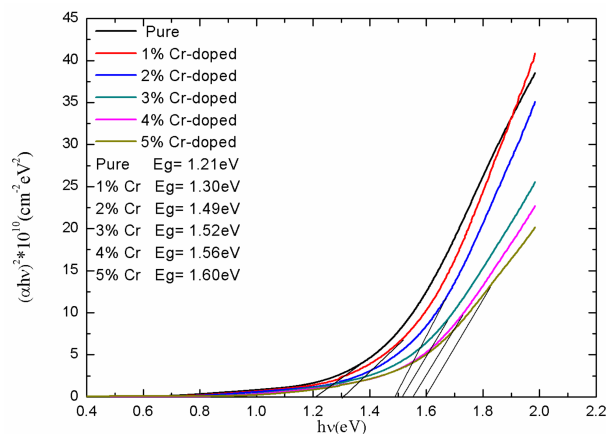


Figure 5. Optical band-gap spectra of the samples as a function of Cr doping.

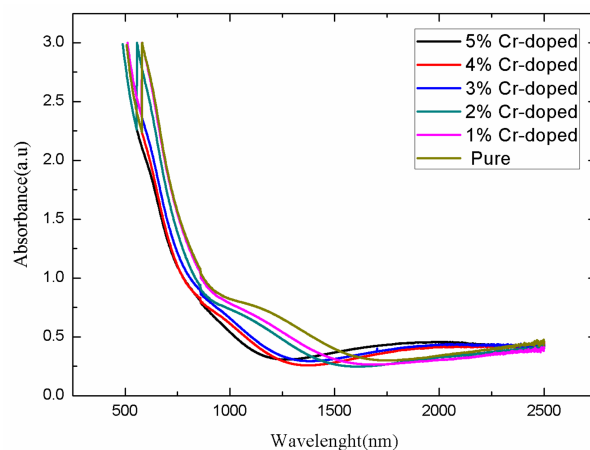


Figure 6. Absorbance spectra of the pure and Cr-doped PbS films.

3.4. Electrical Properties

Table 2 shows the changes in resistivity, carrier mobility, and carrier concentration of undoped and Cr-doped (1%, 2%, 3%, 4%, and 5%) PbS thin films. The Hall effect measurement results showed that the concentration of Cr doping had a significant impact on the electrical properties of PbS films. The prepared PbS films were all P-type, in accordance with previous reports [4]. The carrier concentration and resistivity of undoped PbS films were $3.7 \times 10^{16} \text{ cm}^{-3}$ and $3.47 \times 10^{-1} \Omega\cdot\text{cm}$, respectively. As the doping concentration increased to 2%, the carrier concentration increased to $20.7 \times 10^{16} \text{ cm}^{-3}$ and the resistivity decreased to $1.23 \times 10^{-1} \Omega\cdot\text{cm}$. This trend may be due to the presence of Cr atoms in the PbS structure, which increases the acceptor state. Therefore, it increases hole carrier density in the valence band and causes low resistance at room temperature [29]. Meanwhile, carrier mobility increased with increasing doping concentration, and reached a maximum value of $59.6 \text{ cm}^2 \text{ V}^{-1}\cdot\text{s}^{-1}$, for this reason, the incorporated Cr may be distributed in the form of a simple substance on the grain boundary because the conductivity of Cr is higher than that of Pb. Thus, it helps weaken the electron scattering effect at the grain boundary and leads to an increase in carrier mobility.

At higher Cr doping concentrations, the film carrier concentration will decrease. We believe that, when a small amount of elemental chromium enters the PbS lattice, a large number of carriers are introduced, causing a sharp increase in carrier concentration. However, as elemental Cr amounts increase, they caused a solid-state doping reaction which resulted in a significant increase in the recombination of electrons and holes with a significant drop in carrier concentration. The decrement in carrier mobility can be explained by the reduction in grain size, shown in the XRD diffraction pattern. The grain size decrease led to an increase in grain boundary scatter, thus decreasing the carrier mobility. The increase in resistivity can be attributed to the carrier concentration drop. This explanation was mentioned in previous research [30]. The resistance was minimized with the 2% doped PbS film; this implies it might have application as an absorber material in solar cell devices due to its low power consumption [17].

Table 2. Electrical properties of pure and Cr-doped PbS thin films.

| Cr Content (at.%) | Resistivity ($10^{-1} \Omega\cdot\text{cm}$) | Hall Mobility μ ($\text{cm}^2\cdot\text{V}^{-1}\cdot\text{s}^{-1}$) | Volume Carrier Concentration (10^{16} cm^{-3}) |
|-------------------|--|---|--|
| 0 | 3.47 | 8.27 | 3.70 |
| 1 | 2.95 | 11.9 | 6.86 |
| 2 | 1.23 | 59.6 | 20.7 |
| 3 | 5.43 | 6.18 | 1.53 |
| 4 | 6.9 | 3.9 | 0.659 |
| 5 | 13.2 | 2.15 | 0.304 |

4. Conclusions

This study demonstrated the effect of Cr on the structural and photo/electrical properties and the surface morphology of PbS films for the first time. The structural study showed that Cr^{3+} ions were incorporated into the PbS lattice. The crystallite sizes of the films decreased from 71.5 to 18.9 nm with different dopant levels. Optical absorption data showed that the width of the optical band gap increased from 1.21 to 1.60 eV.

The 2 at.% Cr-doped PbS nanofilm had an excellent XRD pattern and a band gap of 1.49 eV, which allows it to better absorb visible to near-infrared sunlight. Moreover, the 2% doped PbS film had the smallest resistivity compared to the undoped PbS film. In summary, the 2% Cr-doped PbS film has potential use as an excellent absorbent material for solar cells.

Author Contributions: Conceptualization, J.H. and W.L.; Methodology, J.H.; Software, T.W.; Validation, T.W., W.L. and J.H.; Formal Analysis, J.H.; Investigation, W.L.; Resources, W.L.; Data Curation, J.H.; Writing—Original Draft Preparation, J.H.; Writing—Review and Editing, W.L.; Visualization, T.W.; Supervision, W.L.; Project Administration, W.L.; Funding Acquisition, T.W.

Funding: This research was funded by the National Natural Science Foundation of China (Nos. 11674106 and 51505158).

Acknowledgments: We kindly acknowledge financial support from the National Natural Science Foundation of China (Nos. 11674106 and 51505158).

Conflicts of Interest: The authors declare no conflicts of interest.

References

1. Preetha, K.C. Structural, electronic transport and optical properties of Cr doped PbS thin film by chemical bath deposition. In Proceedings of the Let there Be Light: Reflections of a Congress on Light, Kerala, India, 9–11 January 2017.
2. Gaiduk, A.P.; Gaiduk, P.I.; Larsen, A.N. Chemical bath deposition of PbS nanocrystals: Effect of substrate. *Thin Solid Film.* **2008**, *516*, 3791–3795. [[CrossRef](#)]
3. Agrahari, V.; Mathpal, M.C.; Kumar, S.; Kumar, M.; Agarwal, A. Cr modified Raman, optical band gap and magnetic properties of SnO₂ nanoparticles. *J. Mater. Sci. Mater. Electron.* **2016**, *27*, 6020–6029. [[CrossRef](#)]
4. Touati, B.; Gassoumi, A.; Turki, N.K. Structural, optical and electrical properties of Ag doped PbS thin films: Role of Ag concentration. *J. Mater. Sci. Mater. Electron.* **2017**, *28*, 18387–18395. [[CrossRef](#)]
5. Touati, B.; Gassoumi, A.; Dobryden, I.; Natile, M.M.; Vomiero, A.; Turki, N.K. Engineering of electronic and optical properties of PbS thin films via Cu doping. *Superlattices Microstruct.* **2016**, *97*, 519–528. [[CrossRef](#)]
6. Yücel, E.; Yücel, Y. Fabrication and characterization of Sr-doped PbS thin films grown by CBD. *Ceram. Int.* **2017**, *43*, 407–413. [[CrossRef](#)]
7. Yu, K.S.; Shi, J.Y.; Zhang, Z.L.; Liang, Y.M.; Liu, W. Synthesis, characterization, and photocatalysis of ZnO and er-doped ZnO. *J. Nanomater.* **2013**, *2013*, 75. [[CrossRef](#)]
8. Seghaier, S.; Kamoun, N.; Guasch, C.; Zellamac, K. Structural and optical properties of PbS thin films grown by chemical bath deposition. In Proceedings of the Fundamental & Applied Spectroscopy: Second International Spectroscopy Conference, Sousse, Tunisia, 25–28 March 2007.
9. Preetha, K.C.; Murali, K.V.; Ragina, A.J.; Deepa, K.; Dhanya, A.C.; Remadevi, T.L. The role of cationic precursors in structural, morphological and optical properties of PbS thin films. In Proceedings of the National Seminar on Current Trends in Materials Science, Kerala, India, 4–6 August 2011.
10. Thangaraju, B.; Kaliannan, P. Spray pyrolytically deposited PbS thin films. *Semicond. Sci. Technol.* **2000**, *15*, 849–853. [[CrossRef](#)]
11. Kumar, S.; Sharma, T.P.; Zulfequar, M.; Husain, M. Characterization of vacuum evaporated PbS thin films. *Phys. B Phys. Condens. Matter* **2003**, *325*, 8–16. [[CrossRef](#)]
12. Muratore, C. Pulsed laser deposition of thin films, Vol. 2. *Plasma Process. Polym.* **2010**, *4*, 847. [[CrossRef](#)]
13. Asavapiriyant, S.; Chandler, G.K.; Gunawardena, G.A.; Pletcher, D. The electrodeposition of polypyrrole films from aqueous solutions. *J. Electroanal. Chem.* **1984**, *177*, 229–244. [[CrossRef](#)]
14. Gümüş, C.; Ulutaş, C.; Esen, R.; Özkendir, O.M.; Ufuktepe, Y. Preparation and characterization of crystalline MnS thin films by chemical bath deposition. *Thin Solid Film.* **2005**, *492*, 1–5. [[CrossRef](#)]
15. Jana, S.; Thapa, R.; Maity, R.; Chattopadhyay, K.K. Optical and dielectric properties of PVA capped nanocrystalline PbS thin films synthesized by chemical bath deposition. *Phys. E Low Dimens. Syst. Nanostruct.* **2008**, *40*, 3121–3126. [[CrossRef](#)]
16. Seghaier, S.; Kamoun, N.; Brini, R.; Amara, A.B. Structural and optical properties of PbS thin films deposited by chemical bath deposition. *Mater. Chem. Phys.* **2005**, *97*, 71–80. [[CrossRef](#)]
17. Zheng, X.; Fei, G.; Ji, F.; Wu, H.; Zhang, J.; Hu, X.; Xiang, Y. Cu-doped PbS thin films with low resistivity prepared via chemical bath deposition. *Mater. Lett.* **2016**, *167*, 128–130. [[CrossRef](#)]
18. Joshi, R.K.; Sehgal, H.K. Bias-induced changes in carrier type of Pb (1-x) Fe(x)S nanocrystalline solution grown thin films. *J. Cryst. Growth* **2003**, *247*, 425–427. [[CrossRef](#)]
19. Mao, H.-Y.; Lo, S.-Y.; Wu, D.-S.; Wu, B.-R.; Ou, S.-L.; Hsieh, H.-Y.; Horng, R.-H. Hot-wire chemical vapor deposition and characterization of p-type nanocrystalline Si films for thin film photovoltaic applications. *Thin Solid Film.* **2012**, *520*, 5200–5205. [[CrossRef](#)]
20. Williamson, G.K.; Smallman, R.E., III. Dislocation densities in some annealed and cold-worked metals from measurements on the X-ray debye-scherrer spectrum. *Philos. Mag.* **1956**, *1*, 34–46. [[CrossRef](#)]

21. Reddy, T.S.; Kumar, M.C.S. Effect of substrate temperature on the physical properties of co-evaporated Sn₂S₃ thin films. *Ceram. Int.* **2016**, *42*, 12262–12269. [[CrossRef](#)]
22. Yücel, E.; Yücel, Y.; Beleli, B. Optimization of synthesis conditions of PbS thin films grown by chemical bath deposition using response surface methodology. *J. Alloys Compd.* **2015**, *642*, 63–69. [[CrossRef](#)]
23. Portillo, M.C.; Mathew, X.; Santiesteban, H.J.; Castillo, M.P.; Moreno, O.P. Growth and characterization of nanocrystalline PbS:Li thin films. *Superlattices Microstruct.* **2016**, *98*, 242–252. [[CrossRef](#)]
24. Rajashree, C.; Balu, A.R.; Nagarethinam, V.S. Enhancement in the physical properties of spray deposited nanostructured ternary PbMgS thin films towards optoelectronic applications. *J. Mater. Sci. Mater. Electron.* **2016**, *27*, 5070–5078. [[CrossRef](#)]
25. Sadvnikov, S.I.; Gusev, A.I.; Rempel, A.A. Nanostructured lead sulfide: Synthesis, structure and properties. *Russ. Chem. Rev.* **2016**, *85*, 731–758. [[CrossRef](#)]
26. Khot, K.V.; Mali, S.S.; Pawar, N.B.; Mane, R.M.; Kondalkar, V.V.; Ghanwat, V.B.; Patil, P.S.; Hong, C.K.; Kim, J.H.; Heo, J.; et al. Novel synthesis of interconnected nanocubic PbS thin films by facile aqueous chemical route. *J. Mater. Sci. Mater. Electron.* **2014**, *25*, 3762–3770. [[CrossRef](#)]
27. Palominomerino, R.; Portillomoreno, O.; Floresgarcía, J.C.; Hernandez-Tecorralco, J.; Martinez-Juarez, J.; Moran-Torres, A.; Rubio-Rosas, E.; Hernandez-Tellez, G.; Gutierrez-Perez, R.; Chaltel-Lima, L.A. PbS nanostructured thin films by in situ Cu-doping. *J. Nanosci. Nanotechnol.* **2014**, *14*, 5408–5414. [[CrossRef](#)]
28. Thangavel, S.; Ganesan, S.; Chandramohan, S.; Sudhagar, P.; Kang, Y.S.; Hong, C.-H. Band gap engineering in PbS nanostructured thin films from near-infrared down to visible range by in situ Cd-doping. *J. Alloys Compd.* **2010**, *495*, 234–237. [[CrossRef](#)]
29. Gedi, S.; Reddy, V.R.M.; Kang, J.; Jeon, C.-W. Impact of high temperature and short period annealing on SnS films deposited by E-beam evaporation. *Appl. Surf. Sci.* **2017**, *402*, 463–468. [[CrossRef](#)]
30. Choi, H.S.; Jeon, S.; Kim, H.; Shin, J.; Kim, C.; Chung, U.-I. The impact of active layer thickness on low-frequency noise characteristics in InZnO thin-film transistors with high mobility. *Appl. Phys. Lett.* **2012**, *100*, 173501. [[CrossRef](#)]



© 2019 by the authors. Licensee MDPI, Basel, Switzerland. This article is an open access article distributed under the terms and conditions of the Creative Commons Attribution (CC BY) license (<http://creativecommons.org/licenses/by/4.0/>).